CrossMark

Sonochemical Synthesis, Characterization and Sonocatalytic Performance of Terbium-Doped CdS Nanoparticles

Younes Hanifehpour[1] · Nazanin Hamnabard[1] · Babak Mirtamizdoust[2] ·
Sang Woo Joo[1]

Abstract Terbium-doped cadmium sulfide nanoparticles with different terbium contents were successfully synthesized via sonochemical route. The prepared samples were characterized by X-ray diffraction, scanning electron microscopy, photoelectron X-ray spectroscopy, and UV–Vis diffuse reflectance spectroscopy techniques. The as-prepared nanocatalyst were used for sonocatalytic degradation of Methylene Blue. Among the different amounts of dopant, 8 % Tb-doped CdS showed the highest sonocatalytic activity. The order of inhibitory effect of radical scavengers was 1, 4 Benzoquinone $> SO_3^{2-} > CO_2^{3-} > I^-$. The effects of various parameters such as initial dye concentration, catalyst loading, ultrasonic power, and the presence of radical scavengers were investigated.

Keywords Doped CdS · Sonocatalytic degradation · Terbium · Nanocatalyst

✉ Younes Hanifehpour
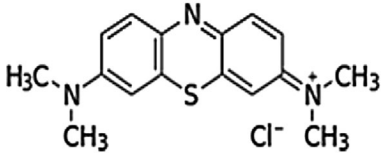   younes.hanifehpour@gmail.com; y_hanifehpour@yu.ac.kr

✉ Babak Mirtamizdoust
   babakm.tamizdoust@gmail.com

✉ Sang Woo Joo
   swjoo1@gmail.com

[1] School of Mechanical Engineering, Yeungnam University, Gyeongsan 712-749, South Korea

[2] Department of Chemistry, Faculty of Science, University of Qom, PO Box 37185-359, Qom, Iran

1 Introduction

Recently, nanocrystalline semiconductors have been broadly studied as the most promising catalyst for environmental remediation processes such as air purification, water purification, heavy metal removal, and hazardous waste remediation because of their high functionality and non-secondary pollution [1–4]. The effects of doping agents and impurities on the physical properties of semiconductors are interesting both for basic and applied research [5–9].

In particular, cadmium sulfide (CdS) with the direct band gap of 2.43 eV, is one of the most important semiconductor and has been given considerable attention by the scientist for potential applications in the future nanodevices, biological labelling and opto-electronics due to tunable electronic band gap depending on the size and shape of nanocrystals. Solar cells, nonlinear optics Light-emitting diodes, photodiodes, and heterogeneous photocatalysis are examples of optoelectronic applications of CdS nanoparticles [10–14].

The fast recombination of generated electron–hole pairs is the drawback that limits the usefulness of semiconductors [15]. This problem can be addressed by doping with metal ions. Metal dopants can act as electron–hole scavengers and increase the lifetime of the charge carriers, and consequently reduce the recombination probability [16, 17]. According to literature reports, metal ion doping of semiconductors has considerably increased the photocatalytic efficiency of these materials [18–20].

In this study, a simple sonochemical route has been introduced for the synthesis of pure and terbium-doped CdS ($Tb_xCd_{1-x}S$) nanoparticles. The sonocatalytic activity of pure and Tb-doped CdS nanoparticles was investigated toward to MB (as a model organic dye) (see Table 1).

Table 1 The characteristic of the dye

Dye name	Chemical structure	Molecular formula	Mw (g/mol)	Dye symbol
Methylene blue		$C_{16}H_{18}N_3SCl$	319.85	MB

Sonication of water promotes the formation, growth, and collapse of small gas bubbles. The collapsing of bubbles in an aqueous solution produces extremely high temperature and pressure conditions called "hot spots". The high temperature near the bubbles leads to thermal decomposition of H_2O molecules to H· and ·OH radicals. These free radicals can directly react with substances near them [21–23]. To the best of our knowledge, no detailed investigation has been reported on the sonocatalytic degradation of MB in the presence of Tb-doped CdS nanoparticles. Other objectives of this work are to investigate the effect of inorganic ions on the decolorization efficiency of methylene blue.

2 Experimental Sections

2.1 Chemicals and Materials

All chemicals used in this study were of analytical grade and were used without further purification. Cd $(NO_3)_2 \cdot 4H_2O$ (99.5 %), $N_2H_4 \cdot H_2O$ (99 %), S (99 %) and NaOH were obtained from Merck; Tb $(NO_3)_3 \cdot 5H_2O$ and ethanol (99 %) were obtained from Sigma-Aldrich. Methylene Blue (MB) was purchased from the Zhejiang Yide Chemical Company (China).

2.2 Synthesis of Tb-Doped CdS Nanoparticles

Tb-doped CdS nanoparticles with variable Tb contents (0–12 mol%) were prepared by sonochemical method using hydrazine hydrate ($N_2H_4 \cdot H_2O$) as the reducing agent. In a typical synthesis, 2 mmol S powder and 1 mmol NaOH and appropriate molar ratios of Tb($NO_3)_3 \cdot 5H_2O$ and Cd($NO_3)_2 \cdot 4H_2O$ were first dissolved in 80 ml distilled water. Under middle speed stirring, hydrazine hydrate ($N_2H_4 \cdot H_2O$) was then added drop wise to the above solution. Finally, the mixture was sonicated for 4 h in a bath type sonicator (SW12H, Fisher Scientific) with a frequency of 35 kHz and output intensity of 100 W. As-synthesized $Tb_xCd_{1-x}S$ nanoparticles were collected and washed with distilled water and absolute ethanol several times in order

to remove residual impurities, and then vacuum-dried at 50 °C for 5 h. The final sombrous yellow powder was obtained as a result.

2.3 Characterization

To determine the crystal phase composition of the prepared CdS and Tb-doped CdS samples, XRD characterization was carried out at room temperature using a D8 Advance, Bruker, Germany diffractometer with monochromatic high-intensity Cu Ka radiation (l = 1.5406 Å), the accelerating voltage of 40 kV and the emission current of 30 mA. SEM (S-4200, Hitachi, Japan) was used to observe the surface state and morphology of the prepared nanoparticles using an electron microscope. The optical absorption spectra of all the samples were recorded using UV–Vis spectrophotometer (Varian Cary 3 Bio, Australia. The chemical composition and evaluation of the chemical state of the final product was performed by X-ray photoelectron spectroscopy (XPS) (K-ALPHA, UK).

2.4 Evaluation of Catalytic Activity

The sonocatalytic activity of pure and Tb-doped CdS nanoparticles was evaluated by the decolorization of MB as a dye pollutant using an ultrasonic bath. In a typical process, 0.1 g of the nanocatalyst was suspended into 100 mL of model dye aqueous solution with a known initial concentration (2.5 mg/L MB). Then, the suspended solution was irradiated by an ultrasonic bath. At time intervals of 10 min, a 3 mL of sample was withdrawn from the ultrasonic reactor, and the residual concentration of MB in the solution after separation of catalyst was measured by spectrophotometer at 655 nm. The color removal was evaluated by determining its absorbance at $\lambda_{max} = 655$ nm by using UV–Vis spectrophotometer. The decolorization efficiency was calculated using Eq. 1:

$$\text{Decolorizatoin efficiency } (\%) = [1 - (C / C_0)] \times 100$$

(1)

where C_o and C are the initial and final concentration of the dye in the solution (mg/L), respectively. In the reusability

test of the nanocatalyst, the used catalyst separated from solution and washed with distilled water and dried at 50 °C and then used in a new experiment.

3 Results and Discussion

Figure 1 shows the powder X-ray diffraction (P-XRD) patterns of the pure and Tb-doped CdS samples. The XRD pattern of pure CdS powders shows peaks at $2\theta = 24.9°$, 26.6°, 28.3°, 36.8°, 43.9°, 48.1°, 51.1°, 52.1°, 53.1°, 54.9°, 58.6°, 67.1°, 69.6°, 71.2°, 72.8° and 75.9° which can be index to (100), (002), (101), (102), (110), (103), (200), (112), (201), (004), (202), (203), (210), (211), (114) and (105) planes. All the diffraction peaks of the samples can be readily indexed to the pure typical well-crystallized hexagonal CdS (JCPDS No. 10-0454) [24, 25]. No peaks indicating impurities were detected, confirming that the sonochemical method applied in this study was successful in synthesizing the desired samples. Moreover, the sharp

diffraction peaks in the XRD spectra of the synthesized samples show that the synthesized products were highly crystalline. Beyond the doping levels of $x = 0.12$ for Tb^{3+}, additional unknown phases were observed. There is a slight shift to the lower diffraction angles in the 12 % Tb-doped CdS pattern. This observation can be related to the contraction of CdS lattice due to the presence of Tb^{3+} ions that have a smaller radius (0.91 Å) compared with Cd^{2+} ions (0.97 Å).

In order to further clarify the size and shape of the nanoparticles, SEM analyses were carried out. Figures 2 and 3 show the SEM microphotographs of the CdS and Tb-doped CdS samples, respectively. SEM images show the bigger crystalline size of the Tb-doped CdS nanoparticles as compared to pure CdS nanoparticles. This confirms that introduction of Tb^{3+} ions into the CdS lattice increases the aggregation of nanoparticles and consequently increase the size of the particles.

The size distribution of the Tb-doped CdS nanoparticles was found to be in the range of 40–60 nm, which is bigger

Fig. 1 Powder X-ray diffraction pattern of $Tb_xCd_{1-x}S$. **a** x = 0.00, **b** x = 0.08, **c** x = 0.12
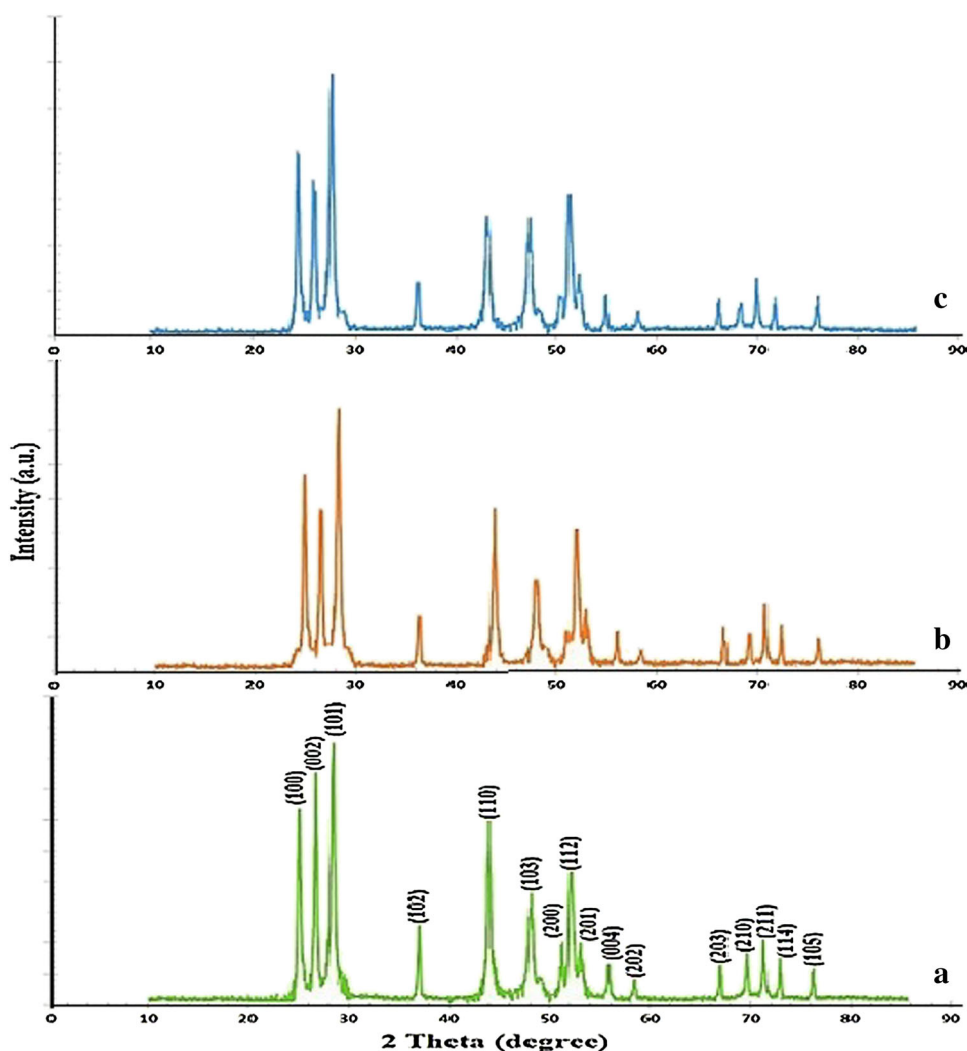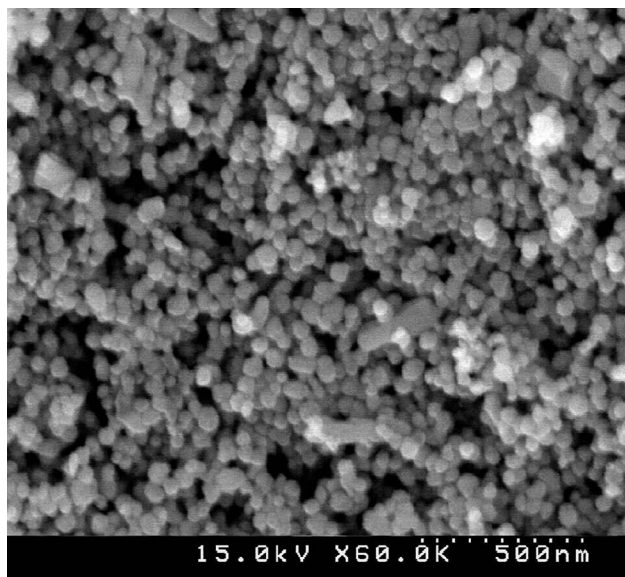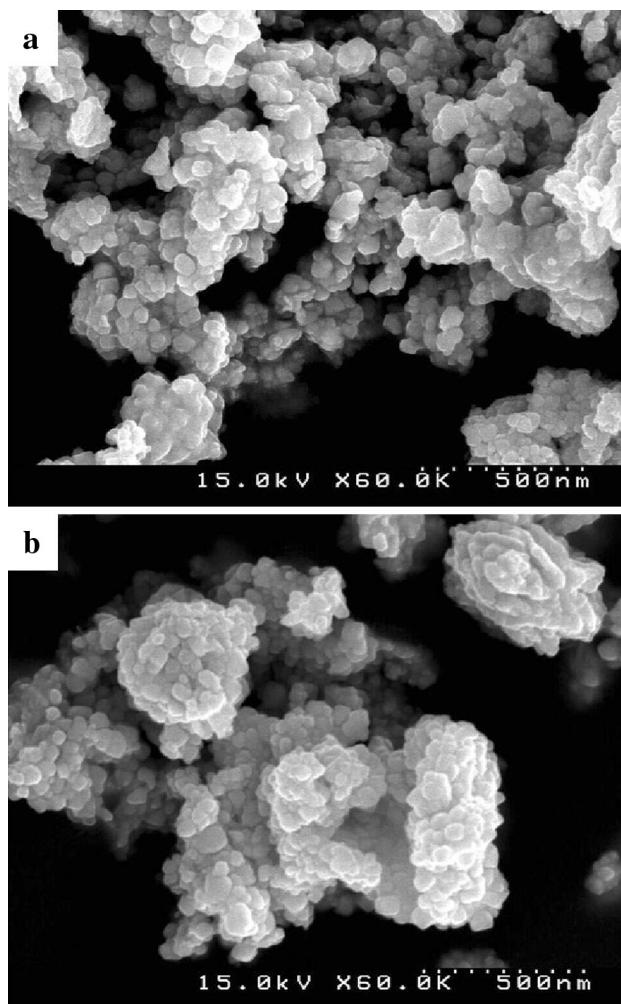
Fig. 2 SEM images of CdS nanoparticles

than that of undoped CdS nanoparticles (20–40 nm) (Fig. 4). These figures confirm that doping of Tb^{3+} into the structure of CdS does not change the morphology of CdS nanoparticles.

XPS analysis of $Tb_{0.08}Cd_{0.92}S$ was performed to confirm the incorporation of Tb ions into the CdS crystal lattice and to investigate the oxidation state of doped Tb. Figure 5a–c shows the XPS spectrum and narrow scan XPS of $Tb_{0.08}Cd_{0.92}S$ nanoparticles. As can be seen in narrow scan spectrum of Cd 3d in Fig. 5a, two peaks centered at 406 and 413 eV can be attributed to the transition of Cd 3d5/2 and Cd 3d3/2, respectively [26]. The S2p spectrum of CdS displays a strong peak at around 163 eV, which is correspond to the coordination of Sulfur and Cd atoms (Cd–S–Cd) in the structure of the hexagonal CdS (Fig. 4b) (see Fig. 5c) [15, 27]. As can be seen in Fig. 5d, the presence of Tb3d peaks located at 1243.56 and 1276.49 eV confirms that Tb ions have been successfully doped into the crystal lattice of CdS [28].

The band gap energy of samples can be evaluated using Tauc plot of $(hv\alpha)^2$ versus (hv) and the intercept of the resulting linear region with the energy axis (Fig. 6). It can be observed that the Eg value of the doped CdS is lower than pure sample, and decreases with the increase of dopant. The band gap energy for pure and Tb-doped CdS is provided at Table 2.

3.1 Effect of Operating Conditions on the Sonocatalysis of Methylene Blue (MB)

The mechanism of sonocatalyses can be explained by means of light and heat energies coming from ultrasonic irradiation. Ultrasonic irradiation combined with CdS

Fig. 3 SEM image of $Tb_{0.04}Cd_{0.96}S$ (a) and $Tb_{0.08}Cd_{0.92}S$ (d) nanoparticles

samples can generate various reactive oxygen species (ROS). Firstly, sonoluminescence caused by ultrasonic irradiation generates light. This excites Tb-doped CdS nanoparticles to act as photocatalysts for the generation of ·OH radicals, as follows [9, 29]:

$$\text{Ultrasonic irradiation} \rightarrow \text{Heat or light} \qquad (2)$$

$$[\text{CdS}] + \text{Heat or light} \rightarrow [\text{CdS}]* \qquad (3)$$

$$[\text{CdS}]* \rightarrow \text{CdS} (h^+ + e^-) \qquad (4)$$

Generated electron–hole pairs react with electron donors and acceptors, then generating active radicals that can react with organic molecules and enhance decolorization efficiency as described by Eqs. (5) and (6):

$$e^- + O_2 \rightarrow O_2^- \qquad (5)$$

$$h^+ + H_2O \rightarrow ·OH + H^+ \qquad (6)$$
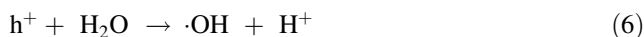
Secondly, the temperature of hot spot by ultrasonic cavitation in aqueous solution can reach higher temperature
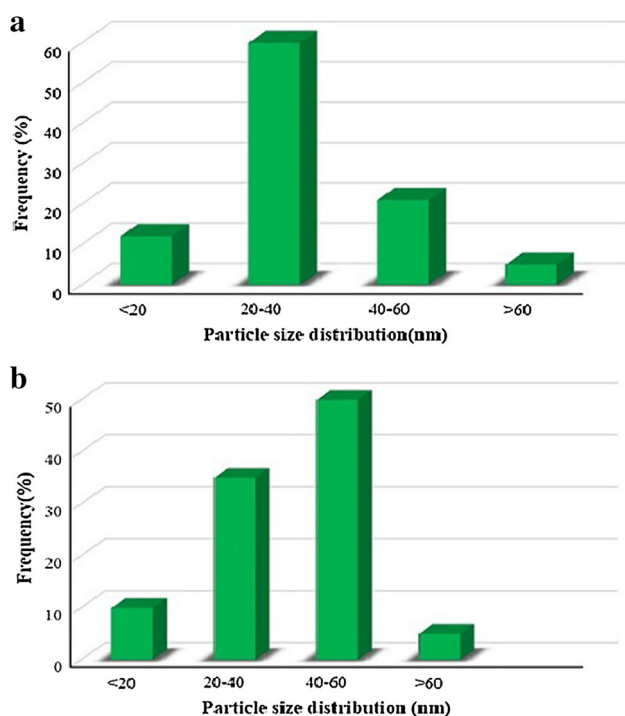
Fig. 4 Size distribution of **a** undoped CdS and **b** 8 % Tb-doped CdS nanoparticles

and higher pressures [29, 30]. Ultrasonic irradiation in the presence of a sonocatalyst generates active radicals, which can decompose the organic pollutant as follows:
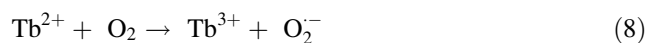
Methylene blue + sonocatalyst + ultrasonic
$\quad\rightarrow$ degradation of dye.

3.1.1 Effect of Tb³⁺ Content of $Tb_xCd_{1-x}S$ Nanoparticles

Figure 7 shows the decolorization efficiency of MB over different Tb-doped CdS sonocatalysts during 80 min of sonolysis. It can be clearly seen that the samples doped with appropriate amount of Tb ion had much higher sonocatalytic activity compared with pure CdS. The highest decolorization efficiency was obtained with 8 % Tb-doped CdS nanoparticles.

The reason for these observations can be explained by two mechanisms. Generally, rare earth metal ions such as Tb^{3+} serve as an electron scavenger and restrain the electron–hole recombination. Also, incorporation of Tb^{+3} ions causes the creation of new energy levels below the conduction band edge of CdS [31–33].

In the case of Tb, with regard to the standard redox potentials of E_0 $(O_2/O_2^{-}) = +0.338$ V, and E_0 $(Tb^{+3}/Tb^{+2}) = -2.8$ V, the presence of Tb^{+3} in crystallite CdS can promote the following reactions [34, 35]:

$$Tb^{3+} + e^{-} \rightarrow Tb^{2+} \tag{7}$$

$$Tb^{2+} + O_2 \rightarrow Tb^{3+} + O_2^{\cdot-} \tag{8}$$

$$O_2^{-} + H^{+} \rightarrow HO\cdot_2 \tag{9}$$

$$2\ HO\cdot_2 \rightarrow H_2O_2 + O_2. \tag{10}$$

$\cdot$OH, H_2O_2 and $O_2\cdot$-radicals are potential oxidants for the degradation of organic pollutants [36, 37].

The changes in the UV–Vis absorption spectra of MB during the sonocatalytic process at different irradiation times are shown in Fig. 8. The decreasing concentration of MB during the sonocatalytic reaction is used to evaluate the activity of the sonocatalyst.

3.1.2 Effect of Catalyst Dosage

To investigate the influence of catalyst dosage on the decolorization efficiency, catalyst dosage was varied between 0.5 and 2 g/L, and the results are displayed in Fig. 9. In this set of experiments, reaction time and initial dye concentration were constant at 80 min and 2.5 mg/L, respectively. As can be seen in Fig. 9, at catalyst concentrations of 0.5, 0.75, 1 and 2 g/L, the color removal efficiency was 49.32, 62.28, 91.23 and 77.31 %, respectively. Thus, decolorization efficiency increased with increasing catalyst dosage from 0.5 to 1 g/L and then decreased. Increasing color removal efficiency with the increase in the amount of sonocatalyst can be attributed to the increasing active surface area for the sonocatalytic degradation of organic dye.

However, beyond 1 g/L, DE % decreases because of the aggregation of sonocatalyst nanoparticles, which reduces the number of active sites and ultrasound scattering, thus hindering the transmission of ultrasound waves in the solution At a low catalyst dosage, the absorption of light controls the sonocatalytic process due to the limited surface area of the catalyst [38].

On the other hand, further increment in the amount of suspended sonoocatalyst led to an increase in the turbidity of the solution and scattering effects, causing the decrease in UV light penetration. This reduces excitement of the sonocatalyst for the generation of OH·. Additionally, the sonocatalyst nanoparticles have a tendency to aggregate at high concentrations, which reduces the number of active sites [39]. Because color removal efficiency decreased with the increase in catalyst dosage from 0.5 to 2 g/L, subsequent experiments were carried out with a catalyst dosage of 1 g/L.

3.1.3 Effect of Initial Dye Concentration

One of the most important parameters influencing sonocatalytic activity is the initial concentration of the target pollutant. In the present work, initial dye concentration was
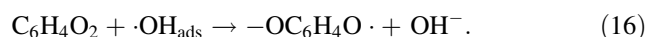
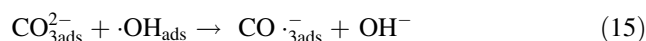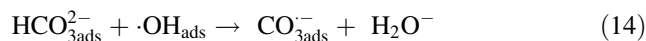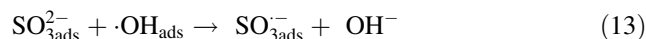**Fig. 5** XPS pattern of 8 % Tb-doped CdS nanoparticles
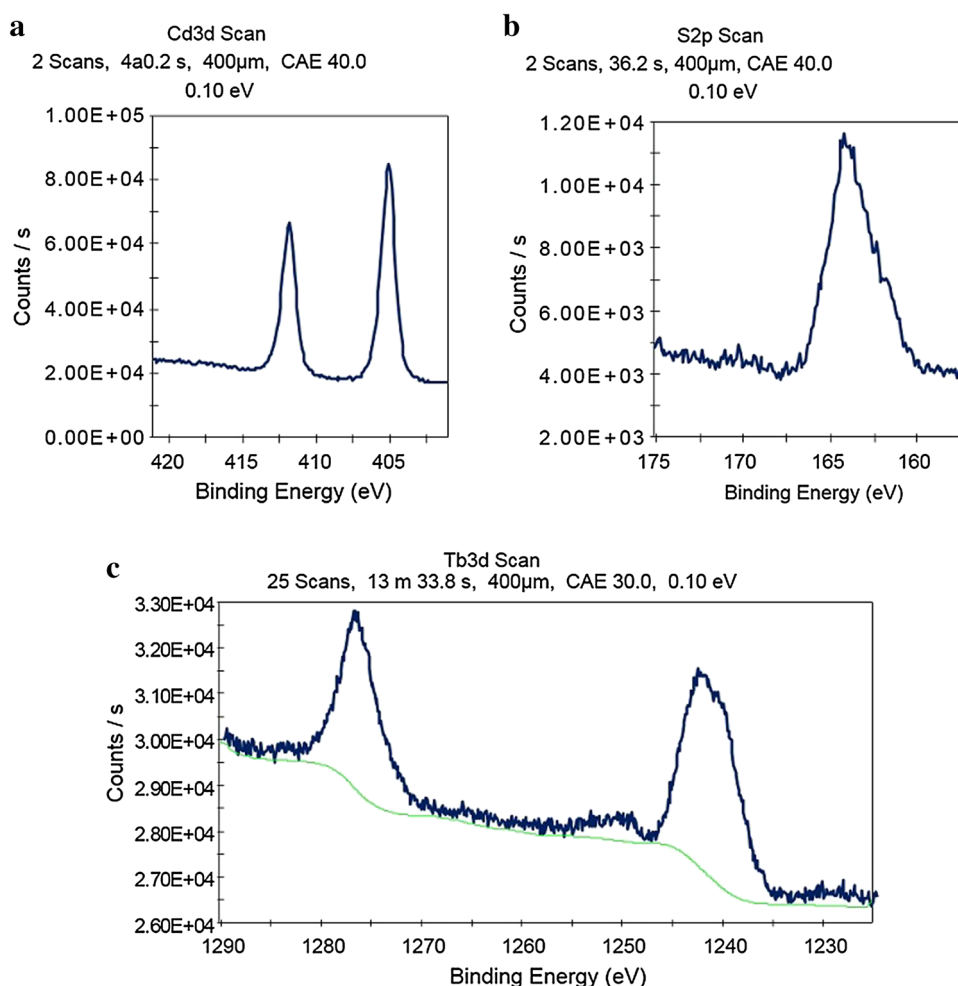
varies between 2.5 and 12.5 mg/L to determine its effect on the decolorization efficiency (Fig. 10). As shown, decolorization efficiency decreased from 91.23 to 20.35 % with an increase in initial concentration from 2.5 to 12.5 mg/L, respectively. This behavior can be attributed to the fact that at high dye concentrations, the active sites on the surface of the sonocatalyst were occupied by the dye molecules, causing a significant decrease in the decolorization efficiency.

In addition, the dye solution becomes dense at a high concentration, which hinders the penetration of light to the catalyst's surface [31]. Hence, the sonocatalytic degradation process is more effective at lower contaminant concentration.

### 3.1.4 Effect of Radical Scavengers on the Sonocatalytic Activity

The decolorization efficiency of MB in the presence of inorganic ions such as I^-, SO_3^{2-}, CO_3^{2-} and $^-OC_6H_4O^.$ is shown in Fig. 11. Figure 11 shows that, when the NaI, Na_2SO_3, Na_2CO_3, and Benzoquinone are added to the

reaction solution separately, the decolorization efficiency of MB decrease considerably. Thus, all of the inorganic anions inhibit the sonocatalytic degradation of MB. The following ions scavenge the produced hydroxyl radicals as indicated in Eqs. (11)–(16) [9, 40]:

$$I^-_{ads} + h^+_{ads} \rightarrow I^._{ads} \tag{11}$$

$$I_{ads} + I^-_{ads} \rightarrow I^._{ads} \tag{12}$$

$$SO_{3ads}^{2-} + \cdot OH_{ads} \rightarrow SO_{3ads}^{-} + OH^- \tag{13}$$

$$HCO_{3ads}^{2-} + \cdot OH_{ads} \rightarrow CO_{3ads}^{-} + H_2O^- \tag{14}$$

$$CO_{3ads}^{2-} + \cdot OH_{ads} \rightarrow CO^._{3ads} + OH^- \tag{15}$$

$$C_6H_4O_2 + \cdot OH_{ads} \rightarrow -OC_6H_4O \cdot + OH^-. \tag{16}$$
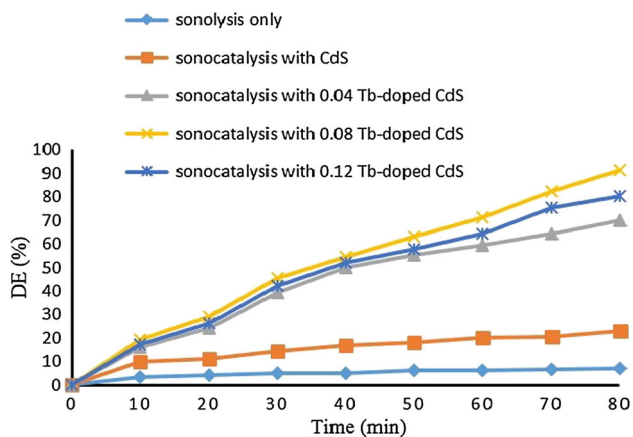
Moreover, the above reactions demonstrate that the CdS surface active sites are blocked by the produced radical anions which are not easily oxidizable, and subsequently the sonocatalytic activity decreases. Consequently, it can be deduced that MB is first absorbed on the surface of the catalyst and then is oxidized under the effect of holes and hydroxyl radicals.

Fig. 6 $(Ah\nu)^2 - h\nu$ curves of the undoped and Tb-doped CdS nanostructures
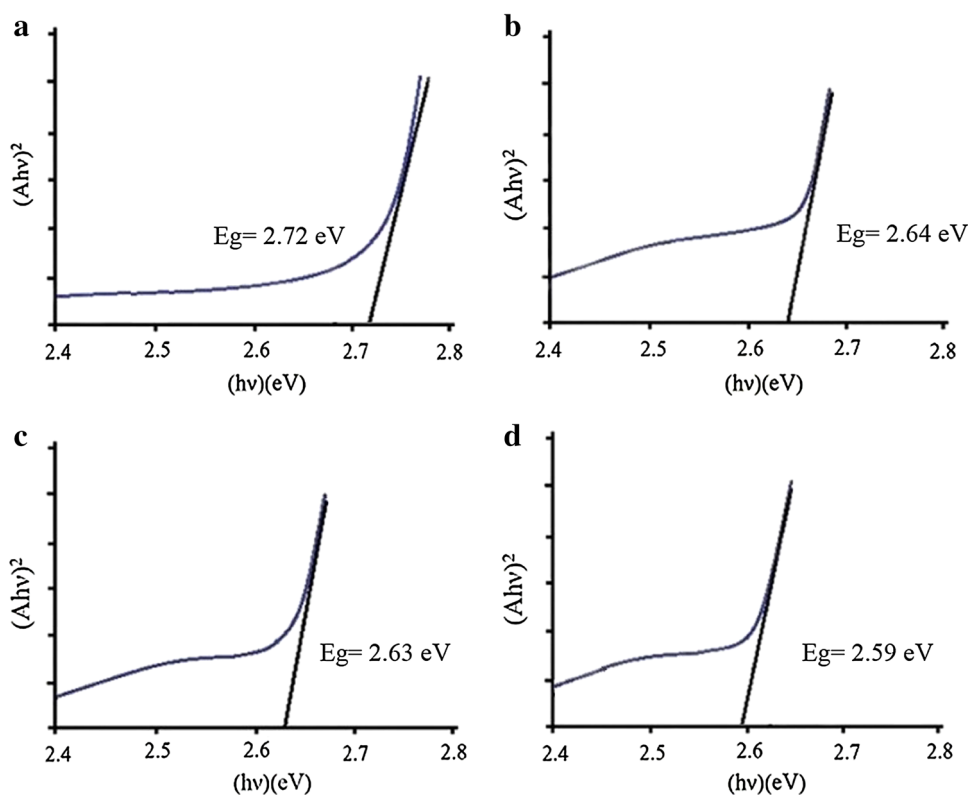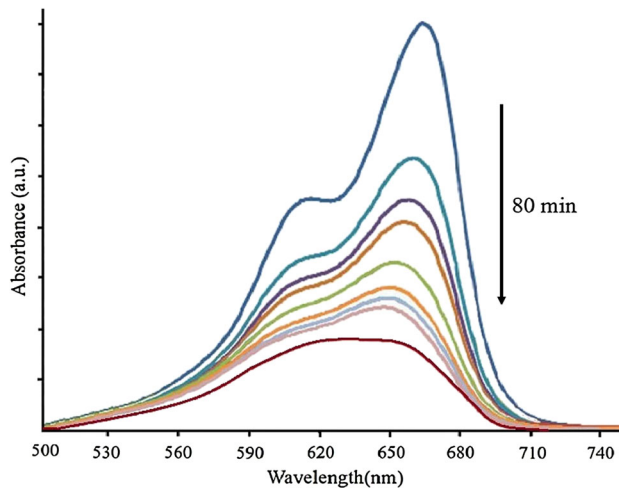

Table 2 Band gap energy of undoped CdS and Tb-doped CdS nanostructures

Sample	Band gap (eV)
Pure CdS	2.72
4 % Tb-doped CdS	2.64
8 % Tb-doped CdS	2.63
12 % Tb-doped CdS	2.59

Fig. 8 Degradation of methylene blue under ultrasonic irradiation using $Tb_{0.08}Cd_{0.92}S$ nanoparticles

3.1.5 Effect of Ultrasonic Power

The ultrasonic power is an important parameter that affects the cavitational activity [41]. Figure 12 shows the sono-catalysis of MB at different ultrasonic powers in the presence of 8 % Tb-doped CdS nanoparticles. By increasing the ultrasound power from 50 to 200 W/L, the degradation efficiency is increased from 68.32 to 100 %.
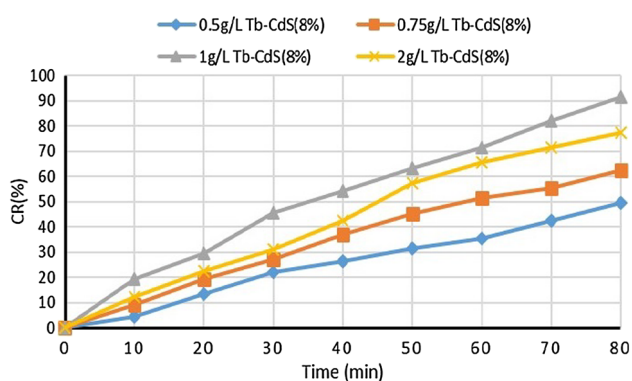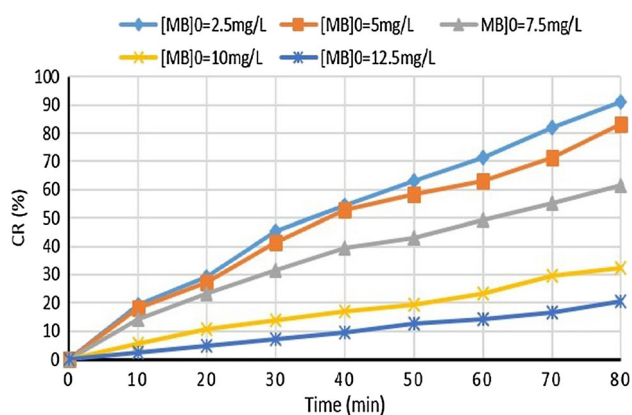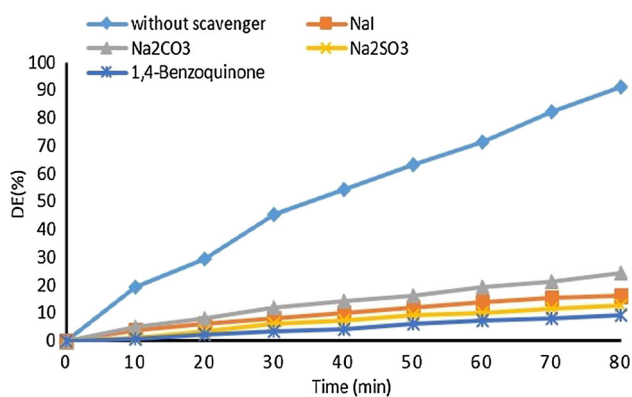

Fig. 7 The effect of Tb^{3+} dopant content on the decolorization of 2.5 mg/L MB (catalyst loading 1 g/L)

Fig. 9 The effect of sonocatalyst loading on the decolorization of 2.5 mg/L MB by the $Tb_{0.08}Cd_{0.92}S$

Fig. 10 The effect of MB concentration on the decolorization of 2.5 mg/L MB ($Tb_{0.08}Cd_{0.92}S$ loading 1 g/L)

Fig. 11 The effect of addition of I^-, CO_2^{3-}, SO_3^{2-} ions and 1, 4 Benzoquinone on the decolorization of 2.5 mg/L MB ($Tb_{0.08}Cd_{0.92}S$ loading 1 g/L)

Due to an increase in the ultrasonic power, it is likely that the net production of the ·OH radicals increases, which results in enhanced decolorization efficiency [42]. In addition, high power increased the turbulence of the solution and thus the mass transfer rate of the dye, reactive

radicals, and intermediates between the surface of the catalyst and bulk solution. The available active sites on the catalyst surface was also increased by the higher de-aggregation of the catalyst [42].

3.2 Reusability of the Sonocatalyst

Reusability is one of the most important factors for a photocatalyst. Figure 13 shows the reusability tests of $Tb_{0.08}Cd_{0.92}S$ sonocatalyst in the decolorization of MB during 5 cycle experiments under optimum conditions, as follows: 2.5 mg/L of MB, 1 g/L of $Tb_{0.08}Cd_{0.92}S$ catalyst, and an irradiation time of 80 min. After each decolorization experiment, the nanocatalyst was washed with distilled water, dried at 60 °C for 5 h, and then used in a new experiment. As shown in Fig. 13, $Tb_{0.08}Cd_{0.92}S$ exhibited excellent chemical stability without any significant decomposition or photocorrosion during the five cycles of photocatalytic reaction. This is an important advantage for practical applications.

4 Conclusion

Pure and Tb-doped CdS were synthesized by a facile sonochemical method and used as a sonocatalyst for degradation of MB via ultrasonic irradiation. The incorporation of Tb ions into the CdS lattice was confirmed by the results of XPS analysis. When doping Tb^{3+} ions into the structure of CdS, the surface morphology of the samples have no obvious changes. The results indicated that the decolorization efficiency of Tb-doped CdS was higher than that of pure CdS. Enhanced decolorization efficiency was observed in the presence of 8 % of dopant. There was an obvious decrease in the decolorization efficiency in the presence of different radical scavengers, including iodide, carbonate, sulfate, and 1,4 Benzoquinone. Consequently,
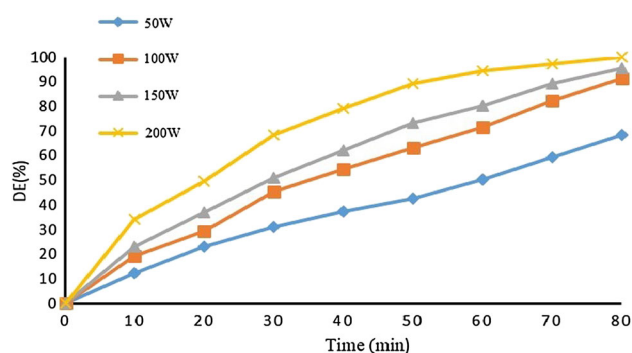
Fig. 12 Effect of ultrasonic power on the sonocatalytic degradation of MB in the presence of 8 % Tb-doped CdS. [MB]0 = 2.5 mg/L, [Catalyst]0 = 1 g/L
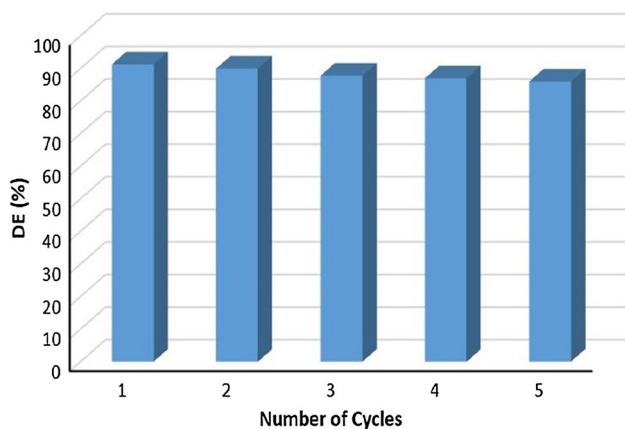
Fig. 13 Reusability of the 8 % Tb-doped CdS nanostructures within five consecutive experimental runs. $[MB]_0 = 2.5$ mg/L, $[Catalyst]_0 = 1$ g/L, the ultrasonic power = 100 W/L, and the reaction time = 80 min

the application of Tb-doped CdS nanoparticles can be an efficient approach for the removal of dye with high reusability potential.

References

1. A.R. Khataee, R. Darvishi, Y. Hanifehpour, M. Safarpour, H. Gholipour, S.W. Joo, Ind. Eng. Chem. Res. **53**, 1924 (2014)
2. A. Fujishima, X. Zhang, D.A. Tryk, Surf. Sci. Rep. **63**, 515 (2008)
3. D.A. Tryk, A. Fujishima, K. Honda, Electrochim. Acta **45**, 2363 (2000)
4. Y. Hanifehpour, B. Soltani, A. Amani-Ghadim, B. Hedayati, B. Khomami, S.W. Joo, J. Ind. Eng. Chem. **34**, 41 (2016)
5. A. Alemi, Y. Hanifehpour, S.W. Joo, B.-K. Min, Colloids. Surf. A. Physicochem. Eng. Asp. **390**, 142 (2011)
6. Y. Hanifehpour, S.W. Joo, B.-K. Min, Nanoscale Res. lett. **8**, 141 (2013)
7. J.H. Park, W.S. Kim, D.-H. Jo, J.S. Kim, J.M. Park, J. Ind. Eng. Chem. **20**, 1965 (2014)
8. A. Khataee, A. Khataee, M. Fathinia, Y. Hanifehpour, S.W. Joo, Ind. Eng. Chem. Res. **52**, 13357 (2013)
9. Y. Hanifehpour, B. Soltani, A. Amani-Ghadim, B. Hedayati, B. Khomami, S.W. Joo, Mater. Res. Bull. **76**, 411 (2016)
10. J. Park, S. Kim, Y. Sim, O.J. Yoon, M.S. Han, H.S. Yang, Y.Y. Kim, Y.M. Jhon, J. Kim, M. Seong, J. Alloy. Compd. **659**, 38 (2016)
11. L. Yu, D. Wang, D. Ye, Sep. Purif. Tech. **156**, 708 (2015)
12. H.L. Lee, A.M. Issam, M. Belmahi, M.B. Assouar, H. Rinnert, M. Alnot, J. Nanomater. **2009**, 41 (2009)
13. R. Banerjee, R. Jayakrishnan, P. Ayyub, J. Phys. **12**, 10647 (2000)
14. M. Acar, E. Bozkurt, K. Meral, M. Arık, Y. Onganer, J. Lumin. **157**, 10 (2015)
15. S. Rehman, R. Ullah, A. Butt, N. Gohar, J. Hazard. Mater. **170**, 560 (2009)
16. N. Hamnabard, Y. Hanifehpour, B. Khomami, S.W. Joo, Mater. Lett. **145**, 253 (2015)
17. M. Wang, C. Huang, Z. Huang, W. Guo, J. Huang, H. He, H. Wang, Y. Cao, Q. Liu, J. Liang, Opt. Mater. **31**, 1502 (2009)
18. C. Liang, C. Liu, F. Li, F. Wu, Chem. Eng. J. **147**, 219 (2009)
19. C.-H. Liang, F.-B. Li, C.-S. Liu, J.-L. Lü, X.-G. Wang, Dyes Pigm. **76**, 477 (2008)
20. M. Asiltürk, F. Sayılkan, E. Arpaç, J. Photochem. Photobiol. A Chem. **203**, 64 (2009)
21. L. Zhu, Z.-D. Meng, C.-Y. Park, T. Ghosh, W.-C. Oh, Ultrason. Sonochem. **20**, 478 (2013)
22. A. Khataee, R. Darvishi, A. Karimi, S.W. Joo, Ultrason. Sonochem. **23**, 219 (2015)
23. A. Khataee, A. Karimi, S. Oskoui, R. Darvishi, Y. Hanifehpour, B. Soltani, S.W. Joo, Ultrason. Sonochem. **22**, 371 (2015)
24. S. Wang, S. Yang, C. Yang, Z. Li, J. Wang, W. Ge, J. Phys. Chem. B **104**, 11853 (2000)
25. V. Nogriya, J.K. Dongre, M. Ramrakhiani, B.P. Chandra, Chalcogen. Lett. **5**, 365 (2008)
26. T. Wang, Z. Jin, T. Liu, W. Li, Y. Ni, J. Am. Ceram. Soc. **93**, 1927 (2010)
27. V. Kishorkumar, S.S. Mali, N.B. Pawar, R.R. Kharade, R.M. Mane, V.V. Kondalkar, P.B. Patil, P.S. Patil, C.K. Hong, J.H. Kim, J. Heo, P.N. Bhosale, New J. Chem. **38**, 5964 (2014)
28. M. Shi, C. Zeng, L. Wang, Z. Nie, Y. Zhao, S. Zhong, New J. Chem. **39**, 2973 (2015)
29. J. Wang, Y. Guo, B. Liu, X. Jin, L. Liu, R. Xu, Y. Kong, B. Wang, Ultrason. Sonochem. **18**, 177 (2011)
30. M. Ahmad, E. Ahmed, Z. Hong, W. Ahmed, A. Elhissi, N. Khalid, Ultrason. Sonochem. **21**, 761 (2014)
31. Y.L. Pang, A.Z. Abdullah, S. Bhatia, Desalination **277**, 1 (2011)
32. O. Yayapao, T. Thongtem, A. Phuruangrat, S. Thongtem, J. Alloy. Compd. **576**, 72 (2013)
33. M. Kim, Y. Choi, S.W. Joo, M. Kang, Y. Sohn, Ceram. Int. **40**, 16051 (2014)
34. A.S. Weber, A.M. Grady, R.T. Koodali, Catal. Sci. Technol. **2**, 683 (2012)
35. D.R. Lide, *CRC handbook of chemistry and physics* (Taylor & Francis, Boca Raton, 2006)
36. P.V. Korake, A.N. Kadam, K.M. Garadkar, J. Rare. Earth. **32**, 306 (2014)
37. X. Dongdong, L. Xiaoni, H. Juan, H. Langhuan, J. Rare. Earth. **31**, 1085 (2013)
38. A. Khataee, A. Karimi, R.D. Soltani, M. Safarpour, Y. Hanifehpour, S.W. Joo, Appl. Catal. A **488**, 160 (2014)
39. R. Kitture, S.J. Koppikar, R. Kaul-Ghanekar, S. Kale, J. Phys. Chem. Solid. **72**, 60 (2011)
40. A. Khataee, M. Hosseini, Y. Hanifehpour, M. Safarpour, S.W. Joo, J. Nanosci. Nanotechnol. **14**, 6950 (2014)
41. N. Golash, P.R. Gogate, Ultrason. Sonochem. **19**, 1051 (2012)
42. L. Hou, H. Zhang, L. Wang, L. Chen, Chem. Eng. J. **229**, 577 (2013)